


RESEARCH ARTICLE

Translational Development of a Zr-89-Labeled Inhibitor of Prostate-specific Membrane Antigen for PET Imaging in Prostate Cancer

Sergio Muñoz Vázquez¹, Heike Endepols^{1,2,3}, Thomas Fischer¹, Samir-Ghali Tawadros⁴, Melanie Hohberg¹, Beate Zimmermanns¹, Felix Dietlein^{1,5}, Bernd Neumaier^{2,3}, Alexander Drzezga¹, Markus Dietlein¹, and Klaus Schomäcker¹ 

¹Faculty of Medicine and University Hospital Cologne, Department of Nuclear Medicine, University of Cologne, Kerpener Str. 62 50937, Cologne, Germany

²Faculty of Medicine and University Hospital Cologne, Institute of Radiochemistry and Experimental Molecular Imaging, University of Cologne, Kerpener Str. 62 50937, Cologne, Germany

³Forschungszentrum Jülich GmbH, Institute of Neuroscience and Medicine, Nuclear Chemistry (INM-5), Wilhelm-Johnen-Straße 52428, Jülich, Germany

⁴Faculty of Medicine and University Hospital Cologne, Center for Experimental Medicine (CEM), University of Cologne, Robert-Koch-Straße 10 50931, Cologne, Germany

⁵Department of Medical Oncology, Dana-Farber Cancer Institute, Harvard Medical School, Boston, MA, USA 2021

Abstract

Purpose: We present here a Zr-89-labeled inhibitor of prostate-specific membrane antigen (PSMA) as a complement to the already established F-18- or Ga-68-ligands.

Procedures: The precursor PSMA-DFO (ABX) was used for Zr-89-labeling. This is not an antibody, but a peptide analogue of the precursor for the production of [¹⁷⁷Lu]Lu-PSMA-617. The ligand [⁸⁹Zr]Zr-PSMA-DFO was compared with [⁶⁸Ga]Ga-PSMA-11 and [¹⁸F]F-JK-PSMA-7 *in vitro* by determination of the K_d value, cellular uptake, internalization in LNCaP cells, biodistribution studies with LNCaP prostate tumor xenografts in mice, and *in vivo* by small-animal PET imaging in LNCaP tumor mouse models. A first-in-human PET was performed with [⁸⁹Zr]Zr-PSMA-DFO on a patient presenting with a biochemical recurrence after brachytherapy and an ambiguous intraprostatic finding with [¹⁸F]F-JK-PSMA-7 but histologically benign cells in a prostate biopsy 7 months previously.

Results: [⁸⁹Zr]Zr-PSMA-DFO was prepared with a radiochemical purity $\geq 99.9\%$ and a very high *in vitro* stability for up to 7 days at 37 °C. All radiotracers showed similar specific cellular binding and internalization, *in vitro* and comparable tumor uptake in biodistribution experiments during the first 5 h. The [⁸⁹Zr]Zr-PSMA-DFO achieved significantly higher tumor/background ratios in LNCaP tumor xenografts (tumor/blood: 309 ± 89 , tumor/muscle: 450 ± 38) after 24 h than [⁶⁸Ga]Ga-PSMA-11 (tumor/blood: 112 ± 57 , tumor/muscle: 58 ± 36) or [¹⁸F]F-JK-PSMA-7 (tumor/blood: 175 ± 30 , tumor/muscle: 114 ± 14) after 4 h ($p < 0.01$). Small-animal PET imaging demonstrated *in vivo* that tumor visualization with [⁸⁹Zr]Zr-PSMA-DFO is comparable to [⁶⁸Ga]Ga-PSMA-11 or [¹⁸F]F-JK-PSMA-7 at early time points (1 h p.i.) and that PET scans up to 48 h p.i. clearly visualized the tumor at late time points. A late [⁸⁹Zr]Zr-PSMA-DFO PET scan on a patient with biochemical recurrence (BCR) had demonstrated intensive tracer accumulation in the right (SUV_{max} 13.25, 48 h p.i.) and in the left prostate lobe (SUV max 9.47), a repeat biopsy revealed cancer cells on both sides.

Conclusion: [⁸⁹Zr]Zr-PSMA-DFO is a promising PSMA PET tracer for detection of tumor areas with lower PSMA expression and thus warrants further clinical evaluation.

Key words Zirconium-89 · Prostate carcinoma · Biochemical recurrence · PET imaging · Radiochemistry · Affinity · Cell uptake · Biokinetics

Introduction

In current clinical practice, tumor localization in patients with biochemical recurrence (BCR) of prostate cancer is the most accepted and validated field of application of PET/CT with Ga-68 or F-18- prostate-specific membrane antigen (PSMA) ligands [1–3]. However, in an estimated 20% of patients with biochemical recurrence the tumor will remain undetected with conventional PSMA PET imaging approaches [4–6].

There are two main reasons for this: First, about 5–10% of primary prostate cancers express no PSMA [7, 8]. Second, different tumors can exhibit a marked heterogeneity in the proportion of PSMA-positive cells they contain [9–11].

It cannot be ruled out that weakly PSMA-expressing prostate carcinoma foci are overlooked when using short-lived radionuclides for a PET scan [12]. A negative finding after PSMA PET/CT examinations using Ga-68- or F-18-ligands therefore represents a selection of prostate carcinoma foci with absent or weak PSMA expression. Our aim was to develop a PSMA ligand that can localize BCRs with weak PSMA expression on the basis of late acquisition windows (2 days after injection or later) and hence achieve an improved lesion-to-background ratio. The intention of this study was not to develop an alternative to short-lived radiotracers, but to expand the range of available PET tracers if, despite rising prostate-specific antigen (PSA) values, no convincing tumor detection with Ga-68 or F-18 PSMA tracers is possible. We designed [⁸⁹Zr]Zr-PSMA-DFO for the rare constellation of a BCR, a preceding PSMA-negative scan with Ga-68- or F-18-PSMA ligands, and the preference for metastasis-directed therapy over androgen deprivation therapy.

To this end, we investigated a new PSMA-binding compound that exploits the longer physical half-life (78.41 h) of Zr-89: [⁸⁹Zr]Zr-*N-sucDf*-AMCHA-2NaI-EuK (*N-sucDf*: *N*-succineimidedesferrioxamine, AMCHA: tranexamic acid, 2NaI: 2-naphthyl-alanine, E: glutamic acid, u: urea, K: lysine; [⁸⁹Zr]Zr-PSMA-DFO). The ligand itself is an analogue of the precursor used to prepare [¹⁷⁷Lu]Lu-PSMA-617. The only difference lies in the chelating agent for zirconium binding. While in DFO-PSMA, the chelating agent is *N-sucDf* (blocked temporarily with Fe(III)), in PSMA-617 DOTA is used for this purpose. So in this study, it is not an antibody that was used for Zr-89 labeling but a small molecule.

Previous studies with Zr-89 have focused primarily on antibody-based PET imaging [13, 14], as the physical half-life of this radionuclide fits well with the biological half-life of the commonly used antibody constructs. The radionuclide Zr-89 decays into the stable isotope Y-89 by positron emission (23%) and electron capture (77%). The E_{\max} of 897 keV and the E_{ave} of 396.9 keV of the emitted positrons are low enough to produce PET images of good spatial resolution. The possibly distorting, spontaneous gamma decay of Zr-89 with 908.97 keV photons (99% abundance) can be masked by adjusting the energy window of the PET scanner [15]. The radionuclide has not previously been used to target PSMA-expressing prostate cancer lesions.

Our first aim with this study was to show that the radiotracer can be produced in good radiochemical quality.

The second aim, carried out in the cell biological/biochemical part of the work, was to compare the [⁸⁹Zr]Zr-PSMA-DFO vector with short-lived radiotracers targeting PSMA ([⁶⁸Ga]Ga-PSMA-11, [¹⁸F]F-JK-PSMA-7 [5, 16–18]) with regard to stability, affinity, cell uptake, and internalization in PSMA-positive cells. The structural formulas of the examined radioligands are shown in Fig. 1.

Third, the animal experimental part of the study was designed to test the hypothesis that higher tumor-to-background ratios can be achieved with [⁸⁹Zr]Zr-PSMA-DFO than with the short-lived tracers.

Fourth, [⁸⁹Zr]Zr-PSMA-DFO was to be applied for the first time in a selected patient with BCR as part of the clinical workup.

The key question was whether the results achievable with [⁸⁹Zr]Zr-PSMA-DFO are at least equal or better to those achieved with [⁶⁸Ga]Ga-PSMA-11 and [¹⁸F]F-JK-PSMA-7.

Materials and Methods

PSMA-11, EuK-2NaI-AMCH-N-sucDf-Fe, and disposable cassette kits were produced by ABX (Radeberg, Germany). Water (Ultrapur[®]), hydrochloric acid 30% (Ultrapur[®]), and sodium hydroxide 30% (Suprapur[®]) were obtained from Merck Millipore (Steinheim, Germany). Serum was collected from whole blood in serum separator tubes. Zr-89 in 1 M oxalic acid was supplied by Perkin Elmer and produced by BV Cyclotron VU (Amsterdam, Netherland). Ga-68 was eluted in a solution of 0.1 M HCl from a Ge-68/Ga-68-Generator Eckert & Ziegler Radiopharma (Berlin, Germany). The other chemicals used were acquired from Sigma-Aldrich (Darmstadt, Germany).

Radiolabeling and Complex-Stability Studies

[⁶⁸Ga]Ga-PSMA-11 and [¹⁸F]F-JK-PSMA-7 were labeled according to standard protocols, which have been published elsewhere [18].

The precursor EuK-2NaI-AMCHA-N-sucDf-Fe used for the Zr-89-based PSMA-vector was formed by coupling the pharmacophore EuK to a naphthyl linker and the chelator agent *N-sucDf*-Fe. The *N-sucDf*-Fe moiety functionalized the molecule for labeling with Zr-89. It proved to be a suitable chelator for [⁸⁹Zr]-zirconium [19].

Labeling of the precursor Fe-N-PSMA-DFO with Zr-89 required a multistep procedure due to the presence of Fe(III).

After preparation of the iron-free PSMA-DFO, the radiolabeling procedure was performed by adjusting the pH of a solution of Zr-89 (20–600 MBq) in 1 M oxalic acid to 6.8–7.2 with 1 M sodium carbonate, 0.5 M HEPES (pH 6.8), and 0.25 M sodium acetate (5 mg/1 ml gentisic acid, 50 µl). Once the desired pH had been reached, a known amount of PSMA-DFO (5, 10, or 20 nmol) was added and the reaction was monitored at different incubation times. The sets of results

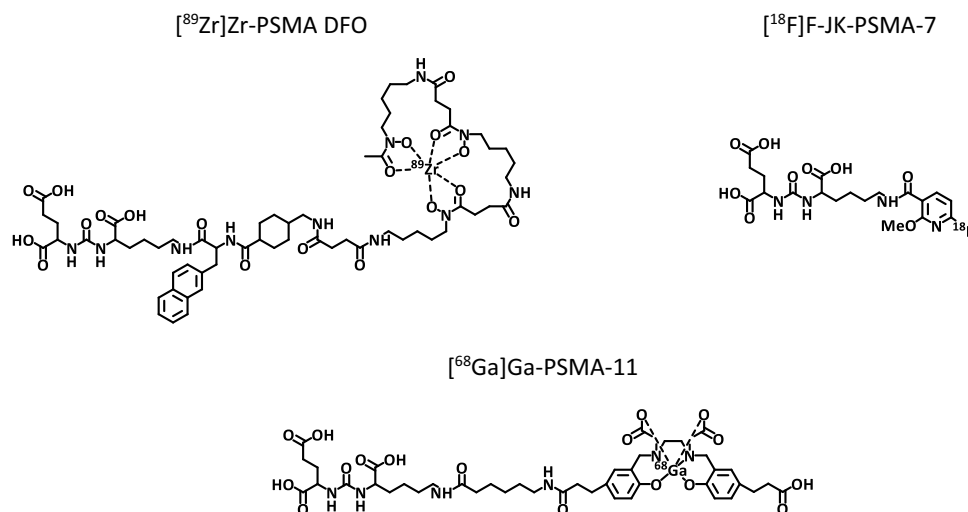


Fig. 1 Structural formulas of the radioligands examined. [⁶⁸Ga]Ga-PSMA-11 and [⁸⁹Zr]Zr-PSMA-DFO contain 3 components: the pharmacophore lysine-urea-glutamate, the chelating agent, and the linker. For [⁶⁸Ga]Ga-PSMA-11, HBED-CC and 6-aminohexanoic (ahx) were used as chelator and linker, respectively. For [⁸⁹Zr]Zr-PSMA-DFO, DFO was used as chelator and naphthylalanine and tranexamic acid (2NaI-AMCHA) were functionalized as linker. In the case of [¹⁸F]F-JK-PSMA-7, the lysine-urea-glutamate scaffold was coupled to tetrafluorophenyl 6-fluoro-4-methoxynicotinate (6-F-4-OMe-Nic-OTfp).

produced by changing the reaction parameters, such as pH, amount of precursor, and incubation time, were evaluated to determine the highest radiochemical yield. The unbound Zr-89 was then efficiently removed by solid-phase extraction using a Sep-Pak™ C₁₈ plus light cartridge.

A complete description of the Zr-89 labeling procedure can be found in the Supplementary information as Supplementary Fig. 1.

To test the release of low molecular weight zirconium species from the PSMA-targeting radiotracer, 100 μl of [⁸⁹Zr]Zr-PSMA-DFO were added to either 1 ml PBS (PAA Laboratories, Pasching Austria) or 1 ml human serum. The solutions were kept at a constant temperature of 37 °C by means of a heating block (Dry Block Heater 1, IKA, Staufen, Germany) for different periods of time after thorough mixing. The samples were checked for radiochemical purity by radio-thin-layer chromatography immediately after reaching a temperature of 37 °C and again after periods of 1 h, 2 h, 24 h, 48 h, and 72 h. The [⁸⁹Zr]Zr-PSMA-DFO remained at the origin of the salicylic acid impregnated instant thin-layer chromatography (ITLC) strip (Agilent, CA, USA), while free Zr-89 migrated with the mobile phase (citrate buffer of 0.5 M pH 5.0). The stability of the complexes was calculated as the percentage of complexes remaining at the origin. The radiochemical purity was additionally determined by HPLC (Column: Macherey–Nagel, NUCLEODUR C₁₈ gravity 5 μm, 110 Å, 250×4 mm) at a flow rate of 1.2 ml/min. Elution with 2 min 5% B was followed by the beginning of the gradient of 5–95% B in 15 min, followed by a hold of 5 min. The A solvent was 0.1% trifluoroacetic acid in water, while 0.1% trifluoroacetic acid in acetonitrile was the B solvent. The unreacted Zr-89 was eluted at retention time $R_t=2.01$ min, while the [⁸⁹Zr]Zr-PSMA-DFO had a $R_t=9.36$ min.

Equilibrium Dissociation Constant K_d

The equilibrium dissociation constant describing the interaction of the radiolabeled ligands with the PSMA binding sites was determined in PSMA-positive LNCaP cell lines (Cell Line Service, Eppelheim, Germany). LNCaP cells were seeded at a density of 10⁶ cells/well on a 6-well plate (Corning, ME, USA) and incubated under 5% CO₂ at 37 °C for 48 h with medium (minimum essential medium Eagle supplemented with 2 mM L-glutamine, 0.1 mM non-essential amino acids (NEAA), 1.0 mM sodium pyruvate, 10% fetal bovine serum, 100 U/ml penicillin, and 100 μg/ml streptomycin) (Lonza, Verviers, Belgium) in a humidified incubator (Thermo Heracell 150 CO₂-Incubator, MA, USA). To determine the nonspecific binding, the medium was removed from selected wells, and 1 ml of a solution of 0.1 mM of 2-(phosphonomethyl)-pentanedioic acid (2-PMPA) in fresh medium was added. 2-PMPA reliably blocks the PSMA binding sites [20, 21]. The plates were then incubated under 5% CO₂, at 37 °C for 1 h. After that, the medium was removed and the cells incubated under the same incubation conditions for 3 h with different concentrations (0.25 nM, 2.5 nM, 5 nM, 10 nM, 25 nM, 50 nM, and 75 nM) of the radiotracer under investigation in 1 ml fresh medium.

After 3 h, the cells were washed three times with 1 ml PBS, and the cells were finally lysed by adding 1 ml of 1 M NaOH and incubating them for 10 min at room temperature. All samples were measured with a gamma counter (Nuklear Medizintechnik Dresden Isomed 100, Dresden, Germany) and were decay-corrected. The equilibrium dissociation constant (K_d) and the maximum density of receptors (B_{max}) were calculated by non-linear regression using GraphPad Prism 8.0.2 (GraphPad Software, San Diego, USA).

Cellular Uptake and Internalization

The cell binding determined in these experiments is the sum of specific and nonspecific cell binding. To determine the values for nonspecific cell binding and internalization, all experiments were additionally performed in the presence of 2-PMPA.

The plates were incubated for 1 h; after which, 0.75 pmol of the radiotracer to be examined was added to 1 ml of fresh medium. The cells were incubated for 30 min, 1, 2, 3, and 5 h. At each time point, the supernatant was removed and the cells washed with 1 ml of PBS. To dissociate the receptor-bound radioligand, the cells were washed twice with 1 ml of a 0.1 M glycine buffer solution at pH 2.8 for 5 min. The 0.1 M glycine-HCl buffer dissociated all the surface-bound complexes. The cells were then washed with 1 ml of PBS, and the internalized fraction was determined by solubilizing the cells with 1 ml of 1 M NaOH and incubating them for 10 min at room temperature. The radioactivity collected from the culture medium, 0.1 M glycine (surface-bound), and 1 M NaOH (internalized fraction) was measured in a gamma counter and decay-corrected. Cell binding was calculated from the surface-bound (0.1 M glycine) and the internalized fraction (1 M NaOH). The internalized fraction was expressed as a percentage of cell binding (internalization to cell-bound radioactivity ratio). All cell uptake experiments were run in triplicate.

Biodistribution in Animal Tissue

After application of the various radiotracers, these experiments were used to determine the radioactivity accumulation in various tissues (percent of the applied radioactivity per gram of organ) and then to calculate tumor/blood, tumor/muscle, tumor/liver, and tumor/kidney ratios.

Animal experiments were performed in strict accordance with the European Union directive 2010/60/EU for animal experiments, and with the approval of the regional authorities (Ministry for Environment, North Rhine-Westphalia).

A total of 35 mice were used for biodistribution experiments. Male CB17-SCID mice (age: 6 weeks, weight: 17–20 g) were purchased from Charles River Laboratories (Wilmington, USA). Mice were kept in groups of 3–5 with free access to water and food in individually ventilated cages (NexGen EcoFlo, cages Mouse500; Allentown Inc., Allentown, NJ, USA) under controlled conditions (22 ± 1 °C and $55 \pm 5\%$ rh) and a 12-h light/dark schedule. The day before implantation of the LNCaP cells, 20 µl of Anti-Asialo GM1 Rabbit (1 mg ml⁻¹ 0.9% NaCl) (FUJIFILM Wako Chemicals GmbH, Neuss, Germany) was injected into each mouse. This was done in order to transiently suppress natural killer cell activity, which is preserved in SCID mice [22]. Tumor cells for implantation were harvested by trypsination (TrypLE™ Express, Life Technologies, Paisley, UK) and 8.7×10^6 cells in 150 µl PBS with Ca²⁺/Mg²⁺ 1:1 with Corning® Matrigel®

matrix (Corning, NY, USA) were inoculated subcutaneously into the right flank of each mouse. After inoculation, the mice were monitored periodically until the cells had formed a tumor of 300 to 600 mg (approximately 6 weeks). The mice were then used either for biodistribution studies or for PET imaging.

On the day of the experiment, each animal was injected intravenously via the tail vein with 30 pmol of [⁸⁹Zr]Zr-PSMA-DFO (approximately 1 MBq/100 µl) or [¹⁸F]F-JK-PSMA-7 (1 MBq/100 µl), or [⁶⁸Ga]Ga-PSMA-11 (1 MBq/100 µl). Five mice were selected for each time point and type of PSMA-targeting radiotracer. The mice were sacrificed by cervical dislocation at 2 and 4 h after injection of [¹⁸F]F-JK-PSMA-7 or [⁶⁸Ga]Ga-PSMA-11 and at 2, 4 and 24 h after administration of [⁸⁹Zr]Zr-PSMA-DFO.

The organs to be studied (blood, liver, spleen, kidneys, muscle, bone, thyroid, lungs, intestines, tumor, heart, and prostate) were dissected out and weighed. The radioactivity in samples was counted in a gamma counter and decay-corrected. The results for each labeled urea-based inhibitor are expressed as a percent of the injected dose per gram of tissue (% ID/g) and presented as means \pm standard deviations (SD) ($n = 5$).

Small-Animal PET in Mice Bearing an LNCaP Tumor Xenograft

PET imaging was used to confirm the results of the biodistribution experiments. [⁶⁸Ga]Ga-PSMA-11 and [¹⁸F]F-JK-PSMA-7 PET (10 MBq of the respective tracer per animal) were acquired for descriptive purposes only. Hence, only one mouse per radiotracer was used for small-animal PET comparisons. The binding specificity of [⁸⁹Zr]Zr-PSMA-DFO was tested using the PSMA blocker 2-PMPA (23 mg/kg, $n = 3$ with and $n = 3$ without 2-PMPA). Scans were conducted under anesthesia on a Focus 220 micro-PET scanner (CTI-Siemens, Germany). Prior to PET imaging, the animals were anesthetized by inhalation of 5% isoflurane/gas mixture (O₂/air 3:7). Thereafter, the anesthesia was reduced and maintained at a concentration of 2% isoflurane/gas mixture.

Emission scans were performed for 60 min, starting 60 min after tracer injection. Additional scans of 60 min duration were performed 4 h, 21 h, and 48 h after injection of [⁸⁹Zr]Zr-PSMA-DFO. All emission scans were followed by a 10-min transmission scan with a Co-57 point source for attenuation correction. Summed images were reconstructed using an iterative OSEM3D/MAP procedure resulting in voxel sizes of 0.47 × 0.47 × 0.80 mm. Post-processing and image analysis was performed with VINCI 4.72 (Max-Planck-Institute for Metabolism Research, Cologne, Germany). Images were Gauss-Filtered (1 mm FWHM) and intensity-normalized to injected dose, corrected for body weight (SUV_{bw}). For this, every frame was divided by injected dose and multiplied by 100 * body weight.

Patient PET/CT Scan

A first-in-human study with [⁸⁹Zr]Zr-PSMA-DFO was performed on a 60-year-old patient with BCR (PSA 3.2 ng/ml, nadir 0.66 ng/ml) as part of the clinical workup. The patient had undergone brachytherapy of the prostate cancer and displayed an increase in PSA level. Seven months previously, [¹⁸F]F-JK-PSMA-7 PET/CT had shown a weak PSMA-positive intraprostatic finding, but a prostate biopsy had contained only histologically benign cells. Findings from a repeat [¹⁸F]F-JK-PSMA-7 PET/CT 7 months later were again ambiguous in the right and left prostate lobe dorsal. After the BCR had failed to be localized by the repeat [¹⁸F]F-JK-PSMA-7 PET/CT, an additional [⁸⁹Zr]Zr-PSMA-DFO PET was recommended as an individual clinical indication. The patient had given his written informed consent for PET imaging and the scientific evaluation of his data. All procedures were performed in accordance with the Institutional Review Board and the regulations of the regional authorities in Cologne. The kidney dose was estimated on the basis of two PET scans. The following assumptions were made for the estimation: Between time 0 (injection) and the first measuring point, the time-activity-curve follows a constant progression. All measuring points were integrated numerically using trapezoidal approximation. From the last measuring point to infinity, a mono-exponential function was fitted and integrated. As the effective half-life could not be accurately determined from two measurement points, the physical half-life of Zr-89 was used instead. Regarding the noise in the [⁸⁹Zr]Zr-PSMA-DFO scans (93 MBq [⁸⁹Zr]Zr-PSMA-DFO versus 343 MBq [¹⁸F]F-JK-PSMA-7), we measured the signal-to-noise ratio (SNR) for all PET/CT scans and the contrast-to-noise ratio (CNR) for the [⁸⁹Zr]Zr-PSMA-DFO-avid lesions and the corresponding areas in the [¹⁸F]F-JK-PSMA-7 PET.

Statistical Analysis

Statistical analyses were performed using GraphPad Prism 8.0.2 (version 8.0.2 for Windows GraphPad Software, San Diego, USA). For the cell uptake experiments, a 2-way ANOVA was performed with the factors radioligand and time point. For the biodistribution experiments, two separate 3-way ANOVA tests were done ([⁸⁹Zr]Zr-PSMA-DFO vs. [⁶⁸Ga]Ga-PSMA-11 and [⁸⁹Zr]Zr-PSMA-DFO vs. [¹⁸F]F-JK-PSMA-7, respectively) with the factors organ, radioligand, and time point. As the 24 h values were available for [⁸⁹Zr]Zr-PSMA-DFO only, this time point was not included in the 3-way ANOVA. To compare the [⁸⁹Zr]Zr-PSMA-DFO 24 h p.i. to the other tracers and other times p.i., a mixed-effects analysis was used for organ uptake, and 1-way ANOVAs for the tumor-to-blood, -kidney- and -muscle ratios. For the PET experiments with the tumor xenograft-bearing mice, three separate 2-way mixed design ANOVA tests (for tumor, liver, and kidneys, respectively) were used with the factors blocking ([⁸⁹Zr]Zr-PSMA-DFO with or without the blocking agent

2-PMPA) and time point (repeated measures). All ANOVA tests were followed by Sidak's or Tukey's multiple comparison procedures. The significance level was always $p < 0.05$.

Results

Radiochemistry and Stability

After the removal of free Zr-89 by solid-phase extraction using a Sep-Pak™ C₁₈ plus light cartridge, the radiochemical purity of [⁸⁹Zr]Zr-PSMA-DFO was $\geq 99.9\%$. The yield of [⁸⁹Zr]Zr-PSMA-DFO in the radiolabeling method was $60.72 \pm 5.50\%$. The molar activity (A_m) reached was 60 MBq/nmol. For comparison, the molar activities of the radioligands used in the following experiments are shown in Table 1.

The Zr-89-radioligand was found to be stable over a period of 7 days at 37 °C in PBS and human serum. The stability test was performed in thin-layer chromatography (TLC) solely to identify free Zr-89 at 1 h, 2 h, 24 h, 48 h, 72 h, and 7 days. However, the stability in PBS was measured in parallel with HPLC at same time intervals, and one single peak was identified at the retention time of [⁸⁹Zr]Zr-PSMA-DFO ($R_t = 9.35$ min).

Affinity, Cell Binding, and Internalization of [⁸⁹Zr]Zr-PSMA-DFO in Comparison with [¹⁸F]F-JK-PSMA-7 and [⁶⁸Ga]Ga-PSMA-11

The radioligands showed no important differences with regard to their *in vitro* behavior when interacting with the LNCaP cells. The binding curves including Scatchard Plots are shown in Supplementary Fig. 2. Table 2 gives an overview of the results of these investigations.

Checking the relationship between B_{\max} and molar activity by linear regression reveals a clear linear relationship: $B_{\max} = 25.37 A_m - 82.63$ ($R^2 = 0.9986$, $p = 0.002$).

The specific binding of radioactively labeled ligands to LNCaP cells, as a percentage of the total activity, ranged between 45.8 and 49.4% after 5 h. The specific internalized activity in LNCaP cells, expressed as a percentage of the cell activity relative to the specific cell-bound activity, was between 58 and 62% after 5 h. More detailed information on the respective values and their statistics can be found in the Supplementary information (Supplementary Tables 1 and 2).

Table 1 Molar activities (A_m) of the radioligands used in the experiments

Radioligand	A_m [MBq/nmol]
[⁸⁹ Zr]Zr-PSMA-DFO	60.4 ± 5.1
[⁶⁸ Ga]Ga-PSMA-11	71.0 ± 9.3
[¹⁸ F]F-JK-PSMA-7	110 ± 15.2

Table 2 Results of investigations on radioligand binding to PSMA-positive LNCaP cells based on Scatchard plots

Radiolabeled ligand	K_d^* [nM]	B_{max}^{**} [fmol/10 ⁶ cells]
[⁸⁹ Zr]Zr-PSMA-DFO	4.97 ± 0.57	1428 ± 42
[⁶⁸ Ga]Ga-PSMA-11	5.15 ± 0.60	1746 ± 53
[¹⁸ F]F-JK-PSMA-7	5.07 ± 0.45	2702 ± 61

* K_d Dissociation constant in nmol** B_{max} Maximum achievable concentration on 10⁶ tumor cells

Biodistribution in Animal Tissue

A 3-way ANOVA was performed to compare organ uptake of [⁸⁹Zr]Zr-PSMA-DFO vs. [⁶⁸Ga]Ga-PSMA-11 and of [⁸⁹Zr]Zr-PSMA-DFO vs. [¹⁸F]F-JK-PSMA-7 (Table 3). Main effects for factor tracer were $F(1,119) = 161.1$; $p < 0.0001$ and $F(1,12) = 48.0$; $p < 0.0001$, respectively, indicating that tracers differed with respect to their biodistribution. Tukey's multiple comparison revealed that the uptake of [⁸⁹Zr]Zr-PSMA-DFO into the LNCaP tumor xenograft was comparable to that of [⁶⁸Ga]Ga-PSMA-11 and [¹⁸F]F-JK-PSMA-7 after 2 h and 4 h. Three ratios were calculated (tumor/blood, tumor/kidney, and tumor/muscle), and a 2-way ANOVA comparison performed on each. Tumor/blood ratios ($F(2,18) = 26.0$; $p < 0.0001$ for factor tracer) were the highest for [⁸⁹Zr]Zr-PSMA-DFO, and significantly different from [⁶⁸Ga]Ga-PSMA-11 at both time points. After 24 h, [⁸⁹Zr]Zr-PSMA-DFO reached the exceptionally high tumor/blood ratio of 309 ± 89 (Table 3). This was confirmed by a

one-way ANOVA, where significant differences were found compared to [⁶⁸Ga]Ga-PSMA-11 and [¹⁸F]F-JK-PSMA-7 with the time points 2 h and 4 h ($F(6,20) = 16.9$, $p < 0.0001$, post hoc $p < 0.05$).

Tumor/kidney ratios ($F(2,18) = 172.7$; $p < 0.0001$) were the highest for [¹⁸F]F-JK-PSMA-7 after 2 h and 4 h, and significantly higher compared to [⁸⁹Zr]Zr-PSMA-DFO, while [⁶⁸Ga]Ga-PSMA-11 tumor/kidney ratios were significantly lower. After 24 h, however, the tumor/kidney ratio of [⁸⁹Zr]Zr-PSMA-DFO (1.0 ± 0.3) surpassed the highest value of [¹⁸F]F-JK-PSMA-7 (0.83 ± 0.13). One-way ANOVA revealed that the tumor/kidney ratio of [⁸⁹Zr]Zr-PSMA-DFO was significantly higher after 24 h than at earlier time points, and compared to [⁶⁸Ga]Ga-PSMA-11 at 2 h and 4 h ($F(6,20) = 38.3$, $p < 0.0001$, post hoc $p < 0.05$).

Tumor/muscle ratios ($F(2,18) = 102.7$; $p < 0.0001$) were highest for [⁸⁹Zr]Zr-PSMA-DFO, and significantly different from [⁶⁸Ga]Ga-PSMA-11 and [¹⁸F]F-JK-PSMA-7 at 2 h and 4 h. After 24 h, tumor/muscle ratio was still 450 ± 38 for [⁸⁹Zr]Zr-PSMA-DFO. One-way ANOVA showed that this was significantly higher compared to [⁶⁸Ga]Ga-PSMA-11 and [¹⁸F]F-JK-PSMA-7 at 2 h and 4 h ($F(6,20) = 62.1$, $p < 0.0001$, post hoc $p < 0.05$).

Tumor/liver ratios ($F(2,10) = 101.7$; $p < 0.0001$) of [⁸⁹Zr]Zr-PSMA-DFO were significantly higher compared to [⁶⁸Ga]Ga-PSMA-11 and [¹⁸F]F-JK-PSMA-7 at 2 h, and significantly higher compared to [¹⁸F]F-JK-PSMA-7 at 4 h. Tumor/liver ratio of [⁶⁸Ga]Ga-PSMA-11 at 4 h was comparable to that of [⁸⁹Zr]Zr-PSMA-DFO. After 24 h, tumor/liver ratio of [⁸⁹Zr]Zr-PSMA-DFO was significantly higher than after 2 h

Table 3 Biodistribution data (%ID/g) of [⁸⁹Zr]Zr-PSMA-DFO, [⁶⁸Ga]Ga-PSMA-11, and [¹⁸F]F-JK-PSMA-7 in CB17-SCID mice bearing LNCaP tumor xenografts ($n = 5$) for each tracer and time point

	[⁸⁹ Zr]Zr-PSMA-DFO			[⁶⁸ Ga]Ga-PSMA-11		[¹⁸ F]F-JK-PSMA-7	
	2 h	4 h	24 h	2 h	4 h	2 h	4 h
LNCaP-tumor	26.3 ± 5.3	22.8 ± 1.5	14.9 ± 1.2	19.4 ± 2.4	23.2 ± 10.6	20.2 ± 2.4	21.3 ± 1.5
Liver	0.95 ± 0.15	0.79 ± 0.17	0.37 ± 0.03	3.17 ± 0.18**	0.65 ± 0.21	4.44 ± 0.78*	3.75 ± 0.50**
Spleen	0.49 ± 0.07	0.61 ± 0.09	0.36 ± 0.08	40.9 ± 9.3**§	62.5 ± 21.5**§	2.15 ± 0.45*	1.57 ± 0.22*
Kidneys	86.7 ± 18.7 [§]	41.3 ± 2.37 [§]	15.4 ± 4.1	231 ± 41 [§]	226 ± 25 [§]	27.2 ± 2.6	26.0 ± 3.5*
Blood	0.14 ± 0.02	0.13 ± 0.04	0.05 ± 0.01	1.34 ± 0.20	0.21 ± 0.03	0.15 ± 0.04	0.12 ± 0.03
Muscle	0.05 ± 0.02	0.08 ± 0.02	0.03 ± 0.01	0.54 ± 0.15	0.42 ± 0.11	0.07 ± 0.02	0.19 ± 0.03
Bone	0.15 ± 0.04	0.13 ± 0.03	0.18 ± 0.02	1.19 ± 0.31	0.50 ± 0.19	0.18 ± 0.03	0.20 ± 0.03
Thyroid	0.18 ± 0.03	0.13 ± 0.02	0.05 ± 0.01	2.13 ± 0.27*	4.44 ± 2.9	0.19 ± 0.02	0.20 ± 0.02
Lung	0.5 ± 0.04	0.12 ± 0.03	0.04 ± 0.01	3.27 ± 1.03	1.23 ± 0.13*	0.18 ± 0.01	0.18 ± 0.04
Intestine	0.65 ± 0.15	0.54 ± 0.10	0.25 ± 0.08	1.50 ± 0.59	0.65 ± 0.30	0.89 ± 0.18	1.53 ± 0.31
Heart	0.11 ± 0.05	0.12 ± 0.03	0.09 ± 0.02	1.10 ± 0.36	1.35 ± 0.70	0.12 ± 0.02	0.10 ± 0.02
Prostate	0.15 ± 0.04	1.12 ± 0.16	0.50 ± 0.01	4.09 ± 1.15	1.67 ± 0.37	0.22 ± 0.03	0.60 ± 0.16
Tumor/blood	183 ± 42 [#]	180 ± 61 [#]	309 ± 89	15 ± 3 [§]	112 ± 57 [§]	142 ± 24 [§]	175 ± 30 [§]
Tumor/kidneys	0.31 ± 0.06 [§]	0.55 ± 0.01 [§]	1.02 ± 0.28	0.09 ± 0.02 ^{§§}	0.10 ± 0.05 ^{§§}	0.74 ± 0.08 ^{**}	0.83 ± 0.13 ^{**}
Tumor/muscle	534 ± 62	297 ± 62 [§]	450 ± 38	37 ± 8 ^{§§}	58 ± 36 ^{§§}	282 ± 71 ^{§§}	114 ± 14 ^{§§}
Tumor/liver	27.5 ± 3.2 [§]	29.6 ± 5.1 [§]	40.0 ± 1.1	6.2 ± 1.0 ^{§§}	34.6 ± 6.6	4.7 ± 1.2 ^{§§}	5.7 ± 0.7 ^{§§}

* $p < 0.05$, ** $p < 0.01$; significantly different from [⁸⁹Zr]Zr-PSMA-DFO uptake at the corresponding time point (three-way ANOVA followed by Tukey's multiple comparisons test for organs, two-way ANOVA for ratios)[#] $p < 0.05$, [§] $p < 0.01$; significantly different from [⁸⁹Zr]Zr-PSMA-DFO uptake at 24 h (two-way ANOVA, mixed-effects model, followed by Tukey's multiple comparisons test for organs, one-way ANOVA for ratios)

and 4 h, and significantly higher than tumor/liver ratio of [⁶⁸Ga]Ga-PSMA-11 and [¹⁸F]F-JK-PSMA-7 at 2 h and [¹⁸F]F-JK-PSMA-7 at 4 h ($F(6,20) = 102.3$; $p < 0.0001$, post hoc $p < 0.05$).

Small-Animal PET in Mice Bearing an LNCaP Tumor Xenograft

The LNCaP tumors were clearly visible with all the tracers tested, when measured for 60 min starting at 1 h p.i. (Fig. 2).

Owing to the longer physical half-life of Zr-89, it was also possible to obtain PET images up to 48 h after injection ($N = 3$, Fig. 3).

The PSMA-inhibitor 2-PMPA markedly reduced the tumor accumulation of the Zr-89-labeled PSMA-targeting vector ($F(1,4) = 10.3$, $p = 0.0324$, post hoc $p < 0.05$ after 1 h). At the same time, the accumulation of radioactivity in the kidneys was also reduced ($F(1,4) = 67.9$, $p = 0.0012$, post hoc $p < 0.05$ after 1 h). Instead, radioactivity accumulated in the liver ($F(1,4) = 2236$, $p < 0.0001$, post hoc $p < 0.05$ after 1 h, 21 h, and 48 h). The clearance of radioactivity from the kidneys was much faster than from the tumor tissue.

[⁸⁹Zr]Zr-PSMA-DFO in a Patient with PCA Recurrence

A first-in-human study was conducted with [⁸⁹Zr]Zr-PSMA-DFO in a 60-year-old patient with BCR (Fig. 4). The [⁸⁹Zr]Zr-PSMA-DFO PET scan demonstrated intensive tracer accumulation in the right prostate lobe dorsal ($SUV_{max} 13.25$, 48 h p.i.) and in the left prostate lobe dorsal ($SUV_{max} 9.47$).

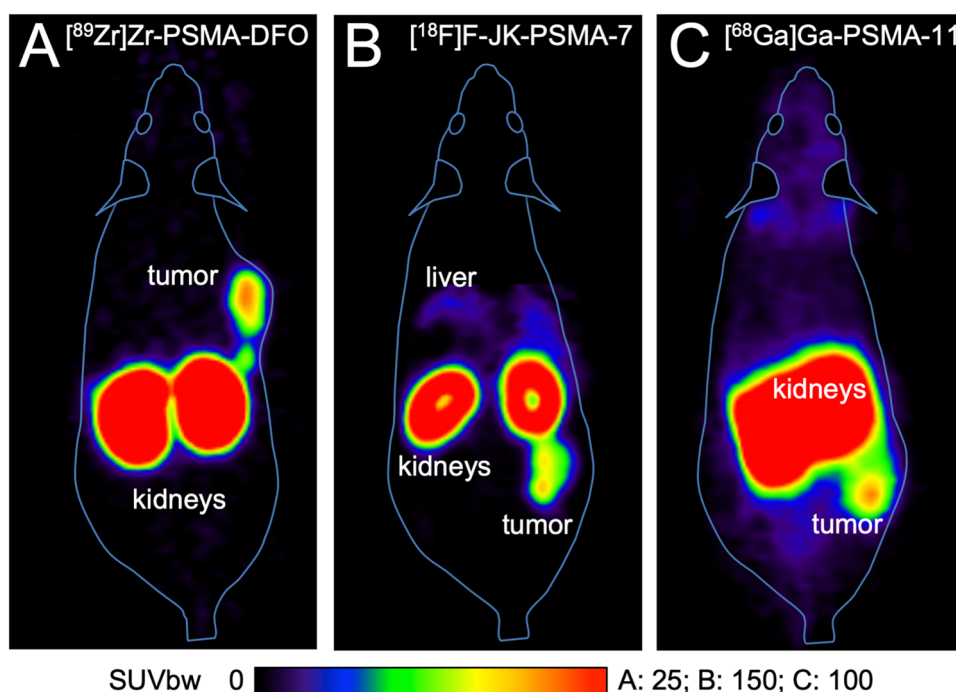
Signal-to-noise ratios (SNR) of [⁸⁹Zr]Zr-PSMA-DFO were 1.9 and 2.0 in the first and second PET scans, respectively. These ratios were lower than those obtained for [¹⁸F]F-JK-PSMA-7 PET at 5.5. However, [⁸⁹Zr]Zr-PSMA-DFO PET/CT exhibited higher contrast-to-noise ratios (CNR) in PSMA-positive lesions (right prostate lobe 3.8 and 3.0 in scans 1 and 2/left prostate lobe 3.5 and 1.1 in scans 1 and 2), compared with [¹⁸F]F-JK-PSMA-7 (right prostate lobe 0.9/left prostate lobe 0.6). This suggests that the detection of the two weak PSMA-avid lesions in our patient was facilitated by the higher CNR of [⁸⁹Zr]Zr-PSMA-DFO. The [⁸⁹Zr]Zr-PSMA-DFO PET scans showed the kidneys to be the organ with the highest radiation exposure. We estimated the kidney dose to be 2.8 mGy/MBq. The overall effective dose (ICRP 60) was 0.11 mSv/MBq. The biopsy was repeated in the light of the intensive PSMA overexpression in the prostate lobes shown by [⁸⁹Zr]Zr-PSMA-DFO PET. The second histopathology revealed cancer cells on both sides and the finding with [⁸⁹Zr]Zr-PSMA-DFO PET was confirmed histopathologically.

Discussion

The following results can be derived from the first radiopharmaceutical, biochemical, and biological data obtained with [⁸⁹Zr]Zr-PSMA-DFO, a PSMA-targeting agent with a longer half-life than Ga-68- or F-18-PSMA ligands, with which it was compared:

1. [⁸⁹Zr]Zr-PSMA-DFO has been produced with high radiochemical purity of > 99%, stability lasting at least

Fig. 2 Whole-body horizontal images (sections) of CB17-SCID mice bearing an LNCaP tumor xenograft with [⁸⁹Zr]Zr-PSMA-DFO (a), [⁶⁸Ga]Ga-PSMA-11 (b), and [¹⁸F]F-JK-PSMA-7 (c), $n = 1$ each. Emission data was acquired 60–120 min p.i.



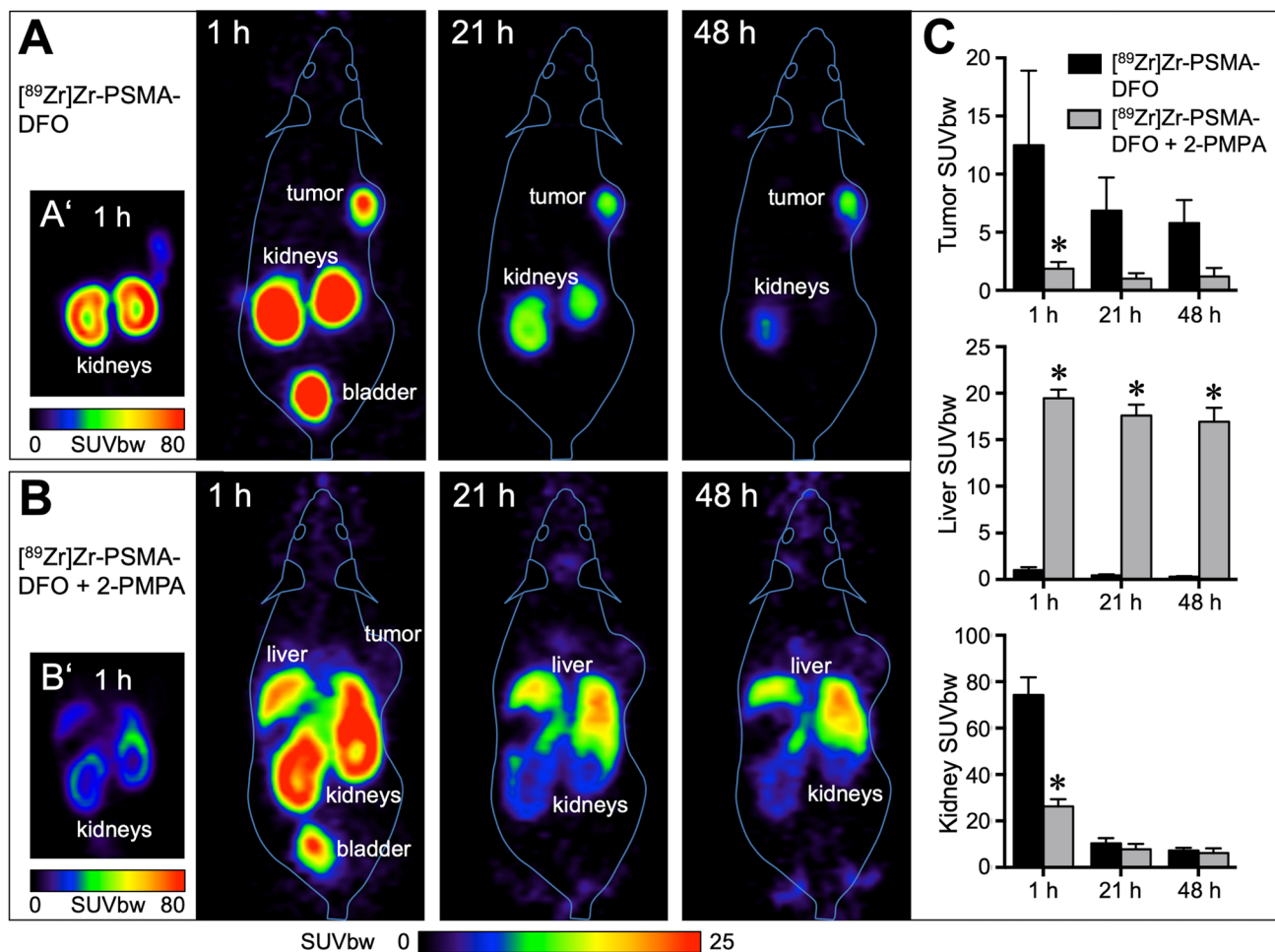


Fig. 3 PET imaging of LNCaP tumor xenografts in mice using [⁸⁹Zr]Zr-PSMA-DFO. **a** Representative image from one of three mice measured at three different time points after injection of 10 MBq [⁸⁹Zr]Zr-PSMA-DFO. Even after 48 h, the LNCaP tumor xenograft was still clearly visible. Residual radioactivity was found in the kidneys and the urinary bladder. In A', kidney radioactivity is shown with a different scaling (SUV_{bw} 0–80 instead of 0–25). **b** Representative image from one of three mice measured at the same time points after injection of 9 MBq [⁸⁹Zr]Zr-PSMA-DFO + 23 mg/kg 2-PMPA. Radioactivity in the tumor was strongly reduced by the addition of 2-PMPA. Instead, radioactivity accumulated in the liver. B' shows that 2-PMPA reduced radioactivity accumulation in the kidneys as well. **c** Quantitative evaluation with *n* = 3 per group. [⁸⁹Zr]Zr-PSMA-DFO uptake in tumor and kidney was significantly reduced with 2-PMPA after 1 h. Radioactivity accumulation in the liver was significantly increased with 2-PMPA at 1 h, 21 h, and 48 h after injection. All images and values are decay-corrected.

- 7 days. Neither the biokinetics nor the examinations using small-animal PET showed a time-dependent increase in Zr-89 accumulation in bone 24 h or 48 h p.i. In view of the known affinity of unchelated zirconium to bone [15, 23, 24], our results indicated a convincing *in vivo* stability.
- The biochemical and biological properties of [⁸⁹Zr]Zr-PSMA-DFO derived from cellular experiments were comparable to those of [⁶⁸Ga]Ga-PSMA-11 and [¹⁸F]F-JK-PSMA-7 during the first 5 h.
- Our preclinical data on [⁸⁹Zr]Zr-PSMA-DFO in LNCaP tumor xenografts in mice demonstrated significantly higher tumor/background ratios after an application interval of 24 h compared with [⁶⁸Ga]Ga-PSMA-11 and [¹⁸F]F-JK-PSMA-7 after an application interval of 2 h or 4 h.

- With [⁸⁹Zr]Zr-PSMA-DFO animal PET, the tumor xenograft remained clearly visible over a prolonged period of 48 h.
- Late PET scans (48 h and 72 h p.i.) in a patient with biochemical relapse indicated a potentially higher contrast-to-noise ratio of [⁸⁹Zr]Zr-PSMA-DFO for localization of tumor areas with a weak PSMA expression on a preceding F-18-labeled PSMA PET.

In the search for a suitable radionuclide for the production of PSMA-targeting ligands, allowing a PET scan to be performed at least 24 h p.i., zirconium-89, which, was considered a promising candidate. The zirconium isotope has become established in immuno-positron emission tomography (PET) imaging in recent years and, with a half-life

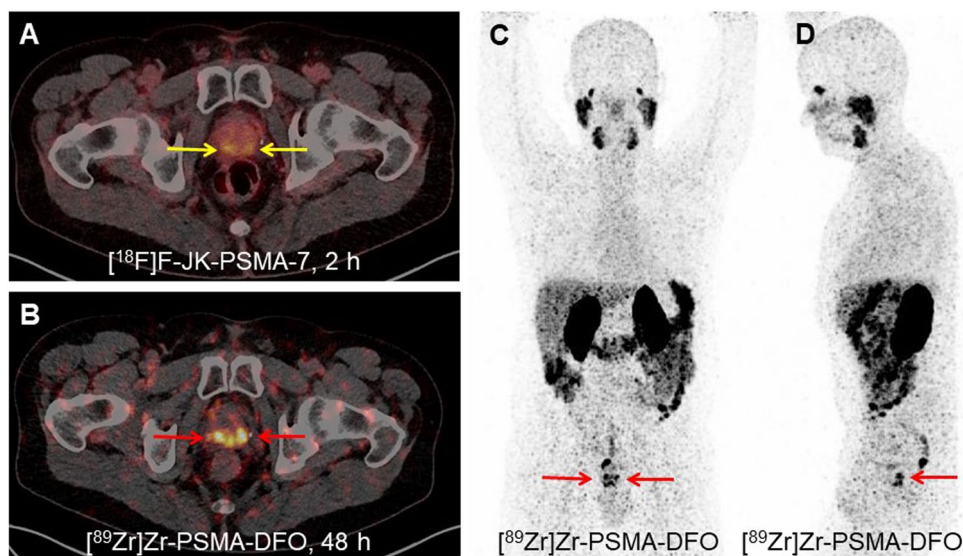


Fig. 4 PET/CT imaging of a histologically confirmed relapse of prostate cancer after brachytherapy. Before the first scan, the patient (Gleason score 3 + 4) received 343 MBq [¹⁸F]F-JK-PSMA-7 and after 6 days 93 MBq [⁸⁹Zr]Zr-PSMA-DFO for the second scan. **a** The [¹⁸F]F-JK-PSMA-7 PET/CT 2 h p.i. was interpreted as equivocal (SUV_{max} 5.37 in the right prostate lobe, 4.63 in the left prostate lobe, yellow arrows) in conjunction with a previously negative biopsy. **b** The additional [⁸⁹Zr]Zr-PSMA-DFO PET scan 48 h p.i. demonstrated intensive tracer accumulation in the right (SUV_{max} 13.25) and in the left prostate lobe (SUV_{max} 9.47) (red arrows). The SUV_{max} values on the PET scan after 72 h were 13.05 in the right prostate lobe and 7.14 in the left prostate lobe. The repeat biopsy revealed cancer cells on both sides. **c, d** The maximum intensity projections (MIP) of the [⁸⁹Zr]Zr-PSMA-DFO PET reveal the PSMA overexpression in the relapse (red arrows) without overlay due to activity in the bladder.

of 3.27 days, meets the requirements better than Cu-64 (0.53 day), Tb-152 (0.73 day), or Sc-44 (0.167 day)—PET radionuclides whose suitability for the production of radioactive PSMA ligands was demonstrated not so long ago [25–29]. The proven high long-term stability of the Zr-89-labeled, PSMA-affine PET tracer in combination with its long half-life also has practical advantages. There is no need to produce the radiopharmaceutical several times a week. Of course, one could argue that nowadays F-18 tracers can also be easily obtained via existing radiopharmaceutical networks in most areas with PET scanners. Nevertheless, the fact that the [⁸⁹Zr]Zr-PSMA-DFO can be stored for a longer period of time and can be applied 7 days after synthesis with a one-off tracer production run speaks for itself. Apart from that, [⁸⁹Zr]Zr-PSMA-DFO can also be transported over longer distances without any major loss of quality.

The labeling procedure, including cleaning and quality control, was feasible within a time frame of about 120 min. The yield based on the Zr-89 activity employed was 75% in optimum cases. After final purification, the radiochemical purity was excellent and remained >99% even on storage in aqueous solution for 7 days.

The linear relationship between the molar activities of the radioactive PSMA vectors examined in this study and their maximum achievable concentration on 10⁶ tumor cells (B_{max}) can be summarized as follows: The higher the molar activity of the radioligand, the more radioligand molecules can be bound to a given number of tumor cells. The assumption derived from this that with higher molar activity, there are

also higher radioactivity concentrations in the tumor tissue and higher tumor-background ratios have not been confirmed (see the “Limitations” section).

Nevertheless, the key question as set out in the introduction, of whether the results obtained with [⁸⁹Zr]Zr-PSMA-DFO correspond to those obtained with [⁶⁸Ga]Ga-PSMA-11 and [¹⁸F]F-JK-PSMA-7 or are better, can be answered as follows: [⁸⁹Zr]Zr-PSMA-DFO showed no inferiority compared to the other PSMA tracers regarding *in vitro* experiments for affinity, binding to prostate cancer tumor cells, and biokinetics.

PSMA-DFO, which serves as an *in vivo* vehicle for Zr-89, is itself a relatively small molecule with faster clearance than, for example, an antibody. This is reflected in the low levels of activity, for example in blood and muscles even at 2 h p.i. The question therefore arises whether it makes sense to combine a relatively long-lived nuclide with a ligand with a short biological half-life. Our cell biological studies showed that [⁸⁹Zr]Zr-PSMA-DFO showed significant internalization. In the context of this work, it can only be assumed that this leads to a re-complexation of the zirconium within the cell and a binding to intracellular molecules. This assumption is supported by a number of studies. Current publications show that Zr-89 is bound intracellularly after it has been able to penetrate the cell wall as a lipophilic complex [30, 31]. Fung et al. [32] observed differences in the clearance rates of radioactivity from the tumor for two forms of the humanized monoclonal antibody J591 ([¹²⁴I]I-J591 and [⁸⁹Zr]Zr-J591) against prostate-specific membrane antigen (PSMA) in mice with LNCaP tumors. So the only difference between

the radioimmunoconjugates was the type of radiolabeling. The authors attribute this difference to typical zirconium trapping mechanisms within the tumor cells which do not operate in the case of non-residualizing of iodine. Similar results were found by Cheal et al. [33] when comparing an antibody against the clear cell renal carcinoma labeled with Zr-89 or I-124. These and other authors conclude that Zr-89 is a residualizing isotope and remains in cells after internalization, allowing activity to accumulate and concentrate in tumor cells while removing non-localized activity from the body, ultimately resulting in high-contrast images.

Our blocking experiment with 2-PMPA showed that in the mouse approximately two-thirds of renal radioactivity is due to specific binding of the PSMA tracer. Around one-third is not blockable, and therefore reflects renal excretion of the radiotracer and its metabolites. Forty-eight hours after injection of [⁸⁹Zr]Zr-PSMA-DFO, there was no detectable radioactivity in the bladder in mice. Thus, Zr-89 is well-suited to detect lesions in the genitourinary tract at late time points, when radioactivity has already cleared from the kidneys and bladder. The scheduling of tracer injection and PET scans on different days was chosen as the optimal arrangement for a few patients with a rare constellation of findings and on account of patient preference.

On the basis of the excellent preclinical imaging properties of [⁸⁹Zr]Zr-PSMA-DFO, we carried out the first observational study on [⁸⁹Zr]Zr-PSMA-DFO PET/CT in a patient with BCR. The activity used (93 MBq) was not derived from a phase-1 trial, but was analogous to the labeling of antibodies with Zr-89 [34]. The first use in humans resulted in a promising performance with regard to clear localization of PSMA-positive tumor tissue when the preceding PET with [¹⁸F]F-JK-PSMA-7 had been interpreted as PSMA-negative or equivocal. The radiation exposure should be weighed against the potential benefit of metastasis-directed therapy or salvage radiotherapy. Additional clinical data in a series of patients will be published in due course and will evaluate whether [⁸⁹Zr]Zr-PSMA-DFO PET can improve the contrast-to-noise ratio in patients with weakly PSMA-positive lesions.

Limitations

Some of the tumor/background ratios determined by measuring the radioactivity of organ samples are unexpected. The highest tumor-muscle ratio was determined just 2 h after the injection of [⁸⁹Zr]Zr-PSMA-DFO. The tumor-to-background ratios for [⁶⁸Ga]Ga-PSMA-11 were significantly lower compared to those of the other radioactive PSMA vectors. It is noticeable that, for example, the tumor/blood ratios given in the literature for [⁶⁸Ga]Ga-PSMA-11 at 2 h p.i. differ widely between individual studies [34–37]. In animal experiments on mice, it should be taken into account that owing to the low blood volume, and variations in the molar activities of the radioactive PSMA ligand used by different authors, different tumor models, or mouse strains can produce different results.

Our work should be seen as a first feasibility study to investigate the suitability of [⁸⁹Zr]Zr-PSMA-DFO for PET examinations of prostate carcinoma lesions with weak PSMA expression. The data collected are not yet sufficient to make generalizable statements about radiation exposure from the radiotracer. This is the subject of a study involving several BCR patients that will be published soon.

Conclusion

This preclinical study demonstrates that the tumor uptake and biodistribution of [⁸⁹Zr]Zr-PSMA-DFO in normal tissues is comparable to that of [⁶⁸Ga]Ga-PSMA-11 and [¹⁸F]F-JK-PSMA-7 in the first 5 h. After an application interval of 24 h, significantly higher tumor/background ratios could be achieved with [⁸⁹Zr]Zr-PSMA-DFO than with [⁶⁸Ga]Ga-PSMA-11 and [¹⁸F]F-JK-PSMA-7 at 2 h and 4 h after application. The first-in-human application in a patient with BCR indicated the potential advantage of [⁸⁹Zr]Zr-PSMA-DFO in the localization of tumors with low PSMA expression on an F-18-labeled PSMA PET. Thus, [⁸⁹Zr]Zr-PSMA-DFO represents a useful addition to the set of PET radiopharmaceutical instruments available for the detection of prostate carcinoma lesions. Clinical investigations of suitable patients with a diagnostic gap in the localization of a biochemical relapse would therefore be worth pursuing.

Supplementary Information The online version contains supplementary material available at <https://doi.org/10.1007/s11307-021-01632-x>.

Funding Open Access funding enabled and organized by Projekt DEAL.

Declarations

Conflict of Interest The authors declare that they have no conflict of interest.

Ethics Approval All applicable institutional and/or national guidelines for the care and use of animals were followed. All procedures performed in studies involving human participants were in accordance with the ethical standards of the institutional and/or national research committee and with the 1964 Helsinki declaration and its later amendments or comparable ethical standards.

Open Access This article is licensed under a Creative Commons Attribution 4.0 International License, which permits use, sharing, adaptation, distribution and reproduction in any medium or format, as long as you give appropriate credit to the original author(s) and the source, provide a link to the Creative Commons licence, and indicate if changes were made. The images or other third party material in this article are included in the article's Creative Commons licence, unless indicated otherwise in a credit line to the material. If material is not included in the article's Creative Commons licence and your intended use is not permitted by statutory regulation or exceeds the permitted use, you will need to obtain permission directly from the copyright holder. To view a copy of this licence, visit <http://creativecommons.org/licenses/by/4.0/>.

References

1. Parikh NR, Tsai S, Bennett C et al (2020) The impact of (18)F-DCFPyL PET-CT imaging on initial staging, radiation, and systemic therapy

- treatment recommendations for veterans with aggressive prostate cancer. *Adv Radiat Oncol* 5:1364–1369
2. Eiber M, Kroenke M, Wurzer A et al (2020) (18)F-rhPSMA-7 PET for the detection of biochemical recurrence of prostate cancer after radical prostatectomy. *J Nucl Med* 61:696–701
 3. Rauscher I, Krönke M, König M et al (2020) Matched-pair comparison of (68)Ga-PSMA-11 PET/CT and (18)F-PSMA-1007 PET/CT: frequency of pitfalls and detection efficacy in biochemical recurrence after radical prostatectomy. *J Nucl Med* 61:51–57
 4. Treglia G, Annunziata S, Pizzuto DA, Giovanella L, Prior JO, Ceriani L (2019) Detection rate of (18)F-labeled PSMA PET/CT in biochemical recurrent prostate cancer: a systematic review and a meta-analysis. *Cancers (Basel)* 11:710
 5. Dietlein F, Hohberg M, Kobe C et al (2020) An (18)F-Labeled PSMA Ligand for PET/CT of prostate cancer: first-in-humans observational study and clinical experience with (18)F-JK-PSMA-7 during the first year of application. *J Nucl Med* 61:202–209
 6. Afshar-Oromieh A, Holland-Letz T, Giesel FL et al (2017) Diagnostic performance of (68)Ga-PSMA-11 (HBED-CC) PET/CT in patients with recurrent prostate cancer: evaluation in 1007 patients. *Eur J Nucl Med Mol Imaging* 44:1258–1268
 7. Ferraro DA, Rüschoff JH, Muehlematter UJ et al (2020) Immunohistochemical PSMA expression patterns of primary prostate cancer tissue are associated with the detection rate of biochemical recurrence with (68)Ga-PSMA-11-PET. *Theranostics* 10:6082–6094
 8. Minner S, Wittmer C, Graefen M et al (2011) High level PSMA expression is associated with early PSA recurrence in surgically treated prostate cancer. *Prostate* 71:281–288
 9. Silver DA, Pellicer I, Fair WR, Heston WD, Cordon-Cardo C (1997) Prostate-specific membrane antigen expression in normal and malignant human tissues. *Clin Cancer Res* 3:81–85
 10. Bravaccini S, Puccetti M, Bocchini M et al (2018) PSMA expression: a potential ally for the pathologist in prostate cancer diagnosis. *Sci Rep* 8:4254–4254
 11. Paschalis A, Sheehan B, Riisnaes R et al (2019) Prostate-specific membrane antigen heterogeneity and DNA repair defects in prostate cancer. *Eur Urol* 76:469–478
 12. Thang SP, Violet J, Sandhu S et al (2019) Poor outcomes for patients with metastatic castration-resistant prostate cancer with low prostate-specific membrane antigen (PSMA) expression deemed ineligible for (177)Lu-labelled PSMA radioligand therapy. *Eur Urol Oncol* 2:670–676
 13. Hafeez U, Parakh S, Gan HK, Scott AM (2020) Antibody-drug conjugates for cancer therapy. *Molecules* 25:4764
 14. Heskamp S, Raavé R, Boerman O, Rijpkema M, Goncalves V, Denat F (2017) (89)Zr-Immuno-positron emission tomography in oncology: state-of-the-art (89)Zr radiochemistry. *Bioconjug Chem* 28:2211–2223
 15. Fischer G, Seibold U, Schirrmacher R, Wängler B, Wängler C (2013) (89)Zr, a radiometal nuclide with high potential for molecular imaging with PET: chemistry, applications and remaining challenges. *Molecules* 18:6469–6490
 16. Brumberg J, Beckl M, Dierks A et al (2020) Detection rate of (68)Ga-PSMA ligand PET/CT in patients with recurrent prostate cancer and androgen deprivation therapy. *Biomedicines* 8:511
 17. Hofman MS (2020) ProPSMA: a callout to the nuclear medicine community to change practices with prospective, high-quality data. *J Nucl Med* 61:676–677
 18. Zlatopolskiy BD, Endepols H, Krapf P et al (2019) Discovery of (18)F-JK-PSMA-7, a PET probe for the detection of small PSMA-positive lesions. *J Nucl Med* 60:817–823
 19. Dewulf J, Adhikari K, Vangestel C, Wyngaert TVD, Elvas F (2020) Development of antibody immuno-PET/SPECT radiopharmaceuticals for imaging of oncological disorders-an update. *Cancers (Basel)* 12:1868
 20. Chatalic KL, Heskamp S, Konijnenberg M et al (2016) Towards personalized treatment of prostate cancer: PSMA I&T, a promising prostate-specific membrane antigen-targeted theranostic agent. *Theranostics* 6:849–861
 21. Kratochwil C, Giesel FL, Leotta K et al (2015) PMPA for nephroprotection in PSMA-targeted radionuclide therapy of prostate cancer. *J Nucl Med* 56:293–298
 22. Dorshkind K, Pollack SB, Bosma MJ, Phillips RA (1985) Natural killer (NK) cells are present in mice with severe combined immunodeficiency (scid). *J Immunol* 134:3798–3801
 23. Abou DS, Ku T, Smith-Jones PM (2011) *In vivo* biodistribution and accumulation of 89Zr in mice. *Nucl Med Biol* 38:675–681
 24. Ghosh S, Sharma A, Talukder G (1992) Zirconium. An abnormal trace element in biology. *Biol Trace Elem Res* 35:247–271
 25. Eppard E, de la Fuente A, Benešová M et al (2017) Clinical translation and first in-human use of [(44)Sc]Sc-PSMA-617 for PET imaging of metastasized castrate-resistant prostate cancer. *Theranostics* 7:4359–4369
 26. Han X-D, Liu C, Liu F et al (2017) (64)Cu-PSMA-617: a novel PSMA-targeted radio-tracer for PET imaging in gastric adenocarcinoma xenografted mice model. *Oncotarget* 8:74159–74169
 27. Cui C, Hanyu M, Hatori A et al (2017) Synthesis and evaluation of [(64)Cu]PSMA-617 targeted for prostate-specific membrane antigen in prostate cancer. *Am J Nucl Med Mol Imaging* 7:40–52
 28. Müller C, Singh A, Umbricht CA et al (2019) Preclinical investigations and first-in-human application of (152)Tb-PSMA-617 for PET/CT imaging of prostate cancer. *EJNMMI Res* 9:68–68
 29. Rosar F, Buchholz H-G, Michels S et al (2020) Image quality analysis of (44)Sc on two preclinical PET scanners: a comparison to (68)Ga. *EJNMMI Phys* 7:16–16
 30. Lechermann LM, Manavaki R, Attili B et al (2020) Detection limit of (89)Zr-labeled T cells for cellular tracking: an *in vitro* imaging approach using clinical PET/CT and PET/MRI. *EJNMMI Res* 10:82–82
 31. Kurebayashi Y, Choyke PL, Sato N (2021) Imaging of cell-based therapy using (89)Zr-oxine ex vivo cell labeling for positron emission tomography. *Nanotheranostics* 5:27–35
 32. Fung EK, Cheal SM, Fareedy SB et al (2016) Targeting of radiolabeled J591 antibody to PSMA-expressing tumors: optimization of imaging and therapy based on non-linear compartmental modeling. *EJNMMI Res* 6:7–7
 33. Cheal SM, Punzalan B, Doran MG et al (2014) Pairwise comparison of 89Zr- and 124I-labeled cG250 based on positron emission tomography imaging and nonlinear immunokinetic modeling: *in vivo* carbonic anhydrase IX receptor binding and internalization in mouse xenografts of clear-cell renal cell carcinoma. *Eur J Nucl Med Mol Imaging* 41:985–994
 34. Lütje S, Franssen GM, Herrmann K et al (2019) *In vitro* and *in vivo* characterization of an (18)F-AIF-labeled PSMA ligand for imaging of PSMA-expressing xenografts. *J Nucl Med* 60:1017–1022
 35. Gourni E, Canovas C, Goncalves V, Denat F, Meyer PT, Maecke HR (2015) (R)-NODAGA-PSMA: a versatile precursor for radiometal labeling and nuclear imaging of PSMA-positive tumors. *PLoS One* 10:e0145755
 36. Umbricht CA, Benešová M, Schmid RM et al (2017) (44)Sc-PSMA-617 for radiotheragnostics in tandem with (177)Lu-PSMA-617-preclinical investigations in comparison with (68)Ga-PSMA-11 and (68)Ga-PSMA-617. *EJNMMI Res* 7:9–9
 37. Ray Banerjee S, Chen Z, Pullambhatla M et al (2016) Preclinical comparative study of (68)Ga-labeled DOTA, NOTA, and HBED-CC chelated radiotracers for targeting PSMA. *Bioconjug Chem* 27:1447–1455